Int J Adv Manuf Technol (2017) 90:2803–2812
DOI 10.1007/s00170-016-9594-0

ORIGINAL ARTICLE

# Boundary conditions optimization of spindle thermal error analysis and thermal key points selection based on inverse heat conduction

Yang Li[1] · Wanhua Zhao[1] · Wenwu Wu[1,2] · Bingheng Lu[1]

Received: 27 May 2016 / Accepted: 10 October 2016 / Published online: 22 October 2016


**Abstract** Thermal error of the spindle is one of the primary contributors of the inaccuracy of the precision machine tools. In order to study the thermal characteristics of the spindle, finite element analysis has been widely used. However, the accuracy of numerical simulation is highly dependent on the boundary conditions especially the coefficients of convection heat transfer. In this paper, the inverse heat conduction theory is introduced and used for optimizing the coefficients of convection heat transfer. Then, the temperature field and thermal error of the spindle are simulated in ANSYS. Based on the simulation results, a new method called mean impact value is proposed to select the thermal key points in the spindle system. Finally, the verification experiments are conducted on a precision horizontal machining center. By comparing the simulation results with the experimental data, the correctness and effectiveness of the heat convection coefficient optimization are verified. In addition, the results of thermal error modeling based on multiple variables including the temperatures of the thermal key points show that the result of the thermal key point selection is satisfying.

**Keywords** Thermal error · Coefficients of convection heat transfer · Thermal key point · Inverse heat transfer · Mean impact value

✉ Wanhua Zhao
whzhao@mail.xjtu.edu.cn

[1] State Key Laboratory for Manufacturing System Engineering, Xi'an Jiaotong University, Xi'an, Shaanxi 710054, China

[2] S.M. Wu Manufacturing Research Center, College of Engineering, The University of Michigan, Ann Arbor, MI 48109-2125, USA

## 1 Introduction

Besides the geometric error, kinematic error, and errors induced by cutting force, tool wear, and chattering, the errors induced by heat which are named as the thermal error are detrimental to the performance of the spindle and the whole machine tool [1–3]. According to the research of Peklenik from Birmingham and Mottu from Geneva, the percentage of the thermal error lies between 40 and 70 % [4].

Spindle is the main component of the machine tool. Its thermal characteristics have great impact on the machining accuracy [5]. In general, there are three ways to reduce the spindle thermal error. These strategies are named as thermal error avoidance, thermal error control, and thermal error compensation [6]. The purpose of thermal error avoidance method is trying to minimize the heat generation or the thermal deformation. Some examples of this method are using symmetric structure and thermally insensitive materials. Thermal error control strategy is supposed to reduce the amount of heat transferred into the spindle system [7, 8]. For example, by placing a layer of thermal insulation material between the bearings and the shaft of the spindle, the heat flowing into the spindle is decreased [9]. Thermal error compensation tends to reduce the thermal error by adjusting the position of the tool and the work piece manually. The first two kinds of methods for reducing the spindle thermal error are always implemented during the designing or assembling phase while the thermal error compensation can be conducted at any phase of the machine tool development even after it has been built.

In order to find out the heat source, to learn the trend and the amount of the temperature change and thermal deformation, and to install the sensors for testing and compensating the spindle thermal error, the spindle thermal characteristics should be analyzed and studied. As the geometric structure of the spindle is three dimensional and the mechanisms of

the heat transfer and the thermoelasticity are complex, it is difficult to obtain the accurate analytical solution of the temperature distribution and the thermal error. It is also a hard, tedious, and time-consuming work to collect enough data from experiments although the practical and real-time thermal performance of the spindle can be obtained through testing. Therefore, numerical analysis is becoming a popular way to investigate the spindle thermal behavior.

Finite element analysis (FEA) is one of the most widely used numerical analysis methods. With help of some commercial FEA software, such as ANSYS, ABAQUS, COMSOL, Marc & Mentat, etc., thermal characteristics of the spindle can be easily obtained [10, 11]. For example, by using ANSYS (workbench module), Creighton [7] simulated the thermal performance of a NSK high-speed micro-milling spindle. According to the FEA results, the temperature of the spindle-motor junction was the highest and the thermal growth of the spindle was 6 μm at the rotation speed of 50,000 RPM. Chen [12] and Zhang [13] also used ANSYS to predict the spindle temperature field and thermal deformation in both steady and transient state. In [14, 15], the thermal performance of the spindle system in a precision boring machine was studied with ABAQUS software. The simulation results indicated that after 11,000 s the spindle reached to the thermal steady state when it was running at 3500 RPM. And the highest temperature of the front bearing and the maximum thermal extension of the spindle were about 53 °C and 35 μm, respectively.

However, the accuracy and the reliability of FEA are closely relied on whether the spindle model is finely meshed and whether the boundary conditions are well defined [16]. In this paper, based on the heat inverse conduction theory, the coefficient of convection heat transfer which is the primary boundary condition is optimized using response surface methodology (RSM). The optimized convection heat transfer coefficients are then applied for simulating the thermal performance of the spindle system in a precision horizontal machining center. The simulation results after and before the optimizations are compared and verified by experiments. In addition, a new thermal key point selection method called mean impact value (MIV) is proposed. Based on the FEA results, the optimized number and positions of sensor for temperature testing are determined. The experimental data of those thermal key points can be further used for building the spindle thermal error model. According to the modeling results, the correctness of the thermal key point selection is verified.

## 2 Boundary conditions optimization based on inverse heat conduction theory

When simulating the thermal characteristics of the spindle, the accuracy of the results is highly dependent on the boundary conditions. The boundary conditions of FEA include the power of heat sources, coefficients of convection heat transfer, fluctuation of environmental temperature, and so on. Among them, the coefficient of convection heat transfer is always considered as the primary one and it is normally calculated according to the traditional functions. In this paper, based on the inverse heat conduction theory, the coefficients of convection heat transfer are firstly optimized and then used to numerically simulate the temperature field and the thermal error of the spindle system.

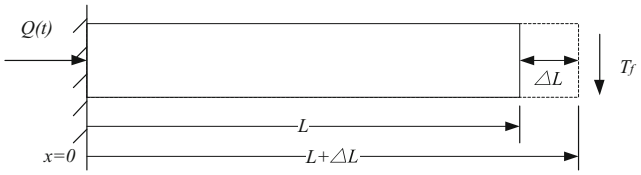


**Fig. 1** 1-D spindle model

### 2.1 Inverse heat conduction problem (IHCP)

All heat transfer problems are focused on the "cause-effect" relationship between the object studied and the environment. Boundary conditions, thermal parameters, initial conditions, and the heat source, etc. are considered as the "causal characteristics." The thermal performance, such as the temperature field is categorized as the "effect." The classical problems of heat transfer, known as the direct problem, are aiming at specifying the cause-effect relationships while the inverse heat transfer problem tends to investigate the causal characteristics from the temperature field information. According to the three main forms of heat transfer, the inverse heat transfer problems are also divided into three groups: inverse heat conduction problem (IHCP), inverse heat convection problem, and inverse heat radiation problem [17].

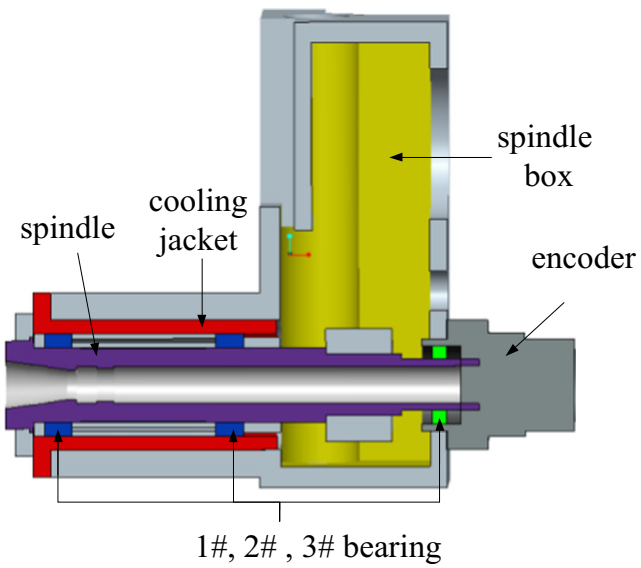


**Fig. 2** Simplified geometrical model of the spindle

**Table 1** Results of convection heat transfer coefficients computation and optimization

| Spindle speed ($r \cdot min^{-1}$) | | Coefficients of convection heat transfer ($W \cdot m^{-2} \cdot K^{-1}$) | | | | | |
|---|---|---|---|---|---|---|---|
| | | Cooling jacket | Spindle shaft | Outer sleeve | Inner sleeve | Encoder | Spindle box |
| 2000 | Before optimization | 267.60 | 56.60 | 39.50 | 54.00 | 60.90 | 5.00 |
| | After optimization | 256.33 | 63.64 | 36.09 | 45.11 | 63.08 | 6.08 |
| 3000 | Before optimization | 267.60 | 74.23 | 54.87 | 75.85 | 79.76 | 5.00 |
| | After optimization | 257.65 | 56.33 | 41.93 | 67.01 | 68.00 | 4.66 |
| 4000 | Before optimization | 267.60 | 89.92 | 69.38 | 95.62 | 96.62 | 5.00 |
| | After optimization | 202.90 | 43.90 | 31.22 | 101.86 | 93.91 | 4.79 |

Inverse heat conduction theory has been widely applied in the field of aerospace, nuclear, chemistry, astrophysics, etc. For example, when the space vehicle was reentering into the atmosphere, the surface temperature of it was too high to be measured directly. By testing the internal temperatures, the heat flux on the surface could be recovered based on the inverse heat conduction theory. It would help engineers to design the shield reasonably [18, 19].

Generally, the spindle system in the machine tool is simplified as the one-dimensional model which is showed in Fig. 1. In the 1-D model, the left end ($x = 0$) is fixed and the other end can be expanded freely when the spindle is heated. It is assumed that the heat ($Q(t)$) flows into the shaft from the left end and then causes the rise of temperature. Meanwhile, the cooling fluid is flowing at the right end and through the heat convection ($q_{conv}$), the spindle is cooled. The temperature of the cooling fluid is $T_f$. Due to the heat effect, the spindle is expanded from $L$ to $L+\triangle L$.

The heat diffusion equation of this model is given by:

$$\frac{\partial^2 \mathrm{T}}{\partial x^2} = \frac{1}{\alpha}\frac{\partial T}{\partial \tau} \tag{1.1}$$

where $T(x, \tau)$ is the temperature distribution of the 1-D spindle at moment $\tau$; $\alpha$ is the thermal diffusivity.

Supposing the initial temperature of the spindle is $T(x, 0) = T_0$, the boundary conditions of this problem are showed as follows.

$$\begin{cases} T = T_0 \ \ \tau = 0 \\ -\lambda\dfrac{\partial T}{\partial x} = \dfrac{Q}{A} \quad x = 0 \\ -\lambda\dfrac{\partial T}{\partial x} = h\left(T - T_f\right) \quad x = L \end{cases} \tag{1.2}$$

where $\lambda$ is the thermal conductivity; $A$ is the cross-section area of the spindle shaft; $h$ is the coefficient of heat convection.

For the 1-D spindle model, the "direct problem" is trying to obtain the temperature field when the cooling fluid temperature ($T_f$), the initial temperature ($T_0$), the heat generation of the bearing (Q(t)), and the coefficient of heat convection ($h$) are all specified. In practical, $T_f$ and $T_0$ are often constant which can also be measured. For certain type of bearing, when its running speed is given, $Q(t)$ is determined. However, $h$ is hard to determine because it is always changed with the temperature and related to the characteristic length ($L$).

In this paper, the "invers problem" is estimating the coefficients of heat convection according to the measured temperature of some certain positions on the spindle.

### 2.2 Optimization of convection heat transfer coefficients

In this paper, response surface methodology (RSM) is applied for optimizing the coefficients of convection heat transfer. RSM is a collection of statistical and mathematical techniques which is popular for optimization studies in the field of chemical, biochemical, medical, and mechanical industries in recent

**Table 2** Material properties of the spindle [23]

| Material | Density ($kg \cdot m^{-3}$) | Modulus of elasticity (GPa) | Poisson's ratio | Specific heat ($J \cdot Kg^{-1} \cdot °C^{-1}$) | Thermal conductivity ($W \cdot m^{-1} \cdot K^{-1}$) | Thermal expansivity ($°C^{-1}$) |
|---|---|---|---|---|---|---|
| 38CrMoALA | 7800 | 208 | 0.28 | 465 | 32.6 | $1.17 \times 10^{-5}$ |
| HT300 | 7600 | 140 | 0.25 | 470 | 39.2 | $1.1 \times 10^{-5}$ |
| GCr15 | 7800 | 208 | 0.28 | 460 | 40.1 | $1.3 \times 10^{-5}$ |
| Steel #45 | 7850 | 200 | 0.3 | 434 | 60.5 | $1.2 \times 10^{-5}$ |

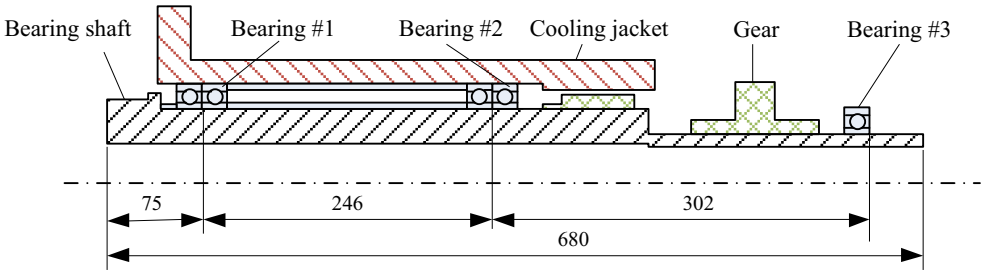


**Fig. 3** Locations of bearings in the spindle system

years [20]. Assuming $x_i$ ($i$ = 1, …, $n$) are the independent variables and $y$ is the response variable. The relationship between them can be written as:

$$y = \mathrm{f}(x_1, x_2, \ldots, x_n) + \varepsilon \tag{1.3}$$

where $\varepsilon$ is the random error.

If the expected response is represented by E($y$) = $\eta$, the surface denoted by $\eta = \mathrm{f}(x_1, x_2, \ldots, x_k)$ is defined as the response surface [21]. In general, the RSM models are divided according to the order of the polynomial of the model. The commonly used model is the second order model, which is showed as follows:

$$\eta = \beta_0 + \sum_{i=1}^{n} \beta_i x_i + \sum_{i=1}^{n} \beta_{ii} x_i^2 + \sum_{1 \le i \le j \le n}^{n} \beta_{ij} x_i x_j \tag{1.4}$$

where $\beta_0$, $\beta_i$, $\beta_{ii}$, and $\beta_{ij}$ are regression coefficients for intercept, linear, quadratic, and interaction coefficients, respectively.

Figure 2 shows the simplified geometrical model of the spindle system in a precision horizontal machining center.

In the spindle system, three sets of bearings are the main heat sources. The air and cooling fluid flows along different components in order to control the temperature rise through heat convection. The effects of radiation are neglected. The coefficients of heat convection are computed according to Eq. 1.5 as follows [22]:

$$h = (Nu \cdot \lambda) \Big/ l \tag{1.5}$$

where $Nu$ is the Nusselt number; $l$ is the characteristic dimension related to the structures of different components. For simplicity, the coefficient of heat convection between the surface of the spindle box and environment is assumed as constant. The value is 5 W/(m$^2$·K).

Then, the coefficients of heat convection between different spindle components and surroundings are optimized using RSM. The computation and optimization results under different working conditions are showed in Table 1.

Applying these optimized convection heat transfer coefficients for simulating the thermal characteristics of the spindle, the accuracy of FEA could be improved. The process and results of the numerical simulation are introduced in Section 3.

## 3 Finite element analysis and thermal key point selection

### 3.1 Numerical simulation of the spindle temperature field and the thermal error

The finite element analysis of the temperature field and thermal error of the spindle is conducted in ANSYS 14.0 (Workbench Module). Firstly, by using sweeping, patch conforming, and automatic method, the simplified spindle model is meshed into 52,469 elements. Then referring to [23], the material properties of the spindle shaft

**Table 3** Parameters and forces loaded on the bearings in the spindle system

| Bearings no. | 1# | 2# | 3# |
|---|---|---|---|
| Type | Angular contact bearing (15°) | Angular contact bearing (15°) | Deep groove ball bearing |
| Model | S71922CD/HCPA9A | S71922CD/HCPA9A | SKF 6015-2R51 |
| Inner ring diameter (mm) | 110 | 110 | 75 |
| Outer ring diameter (mm) | 150 | 150 | 115 |
| Width (mm) | 20 | 20 | 20 |
| Axial force (Fa) (N) | 1034.2 | −1034.2 | 0 |
| Radial force (Fr) (N) | 416.6 | −744.4 | −0.4 |
| Basic static loading rating (N) | 72,000 | 33,500 | 72,000 |

**Table 4** Heat generations of the bearings under different spindle speeds

| Spindle speed (r·min−1) | Heat generation of the bearings (W) | | |
|---|---|---|---|
| | 1# bearing | 2# bearing | 3# bearing |
| 2000 | 279.8 | 280 | 105.8 |
| 3000 | 364 | 364.2 | 138.7 |
| 4000 | 439.1 | 439.4 | 168 |

(38CrMoALA), the spindle box (HT300), bearings (GCr15), and other components (steel #45) are set according to Table 2 .

As shown in Fig. 2, there are three sets of bearings. 1# and 2# bearings are angular contact bearings, and 3# is the deep groove ball bearing. Figure 3 illustrates the locations of these bearings. Parameters of bearings and the force loaded on them (calculated using ROMAX software) are listed in Table 3.

Due to the friction between the balls and races, temperature rises of those bearings are very high. The bearings are considered as the main heat sources in the spindle system. The heat generations of these bearings when the spindle is running at 2000, 3000, and 4000 r/min are computed [24] according to Eq. (1.6). The computing results are showed in Table 4.

$$H_f = 1.047 \times 10^{-4} nM \tag{1.6}$$

where $H_f$ (W) is the heat output of the bearing which is the main heat source; $n$ (r/min) is rotational speed of the bearing; $M$ is the friction torque (N·mm).

The heat generations of bearings are taken as the heat loads. Together with the coefficients of heat convection obtained before, they are applied for numerically simulating the spindle temperature field. In the process of analyzing, the effects of thermal contact resistances are neglected. Figure 4 shows the simulated spindle temperature field in the steady state at 2000 r/min.

From Fig. 4, it can be concluded that compared with other two sets of bearings, temperature of 3# bearing in the steady state (53.9 °C) is higher. This is because that close to 1# and 2# bearings, there are cooling fluids flowing in the cooling jacket, which prevent bearings and the spindle from overheating. But 3# bearing is placed at the end of the spindle system and there is no cooling system. Besides, the temperature of the encoder which is close to 3# bearing is also high. The temperature distribution of spindle box is uniform and the temperature change is not obvious.

The simulation results of the temperature distribution are then applied for static structure FEA to predict the thermal error of the spindle. Figure 5 shows the expected thermal error of the spindle in different directions under the speed of 2000 r/min.

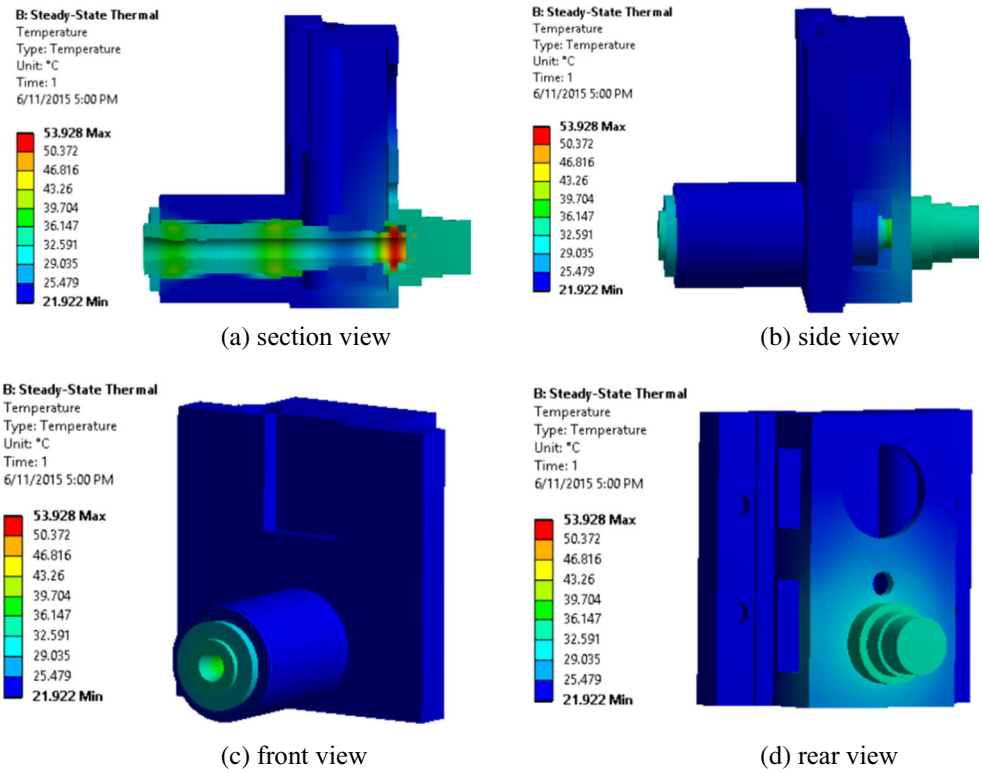


**Fig. 4** Simulated temperature field of the spindle at 2000 r/min (steady state)

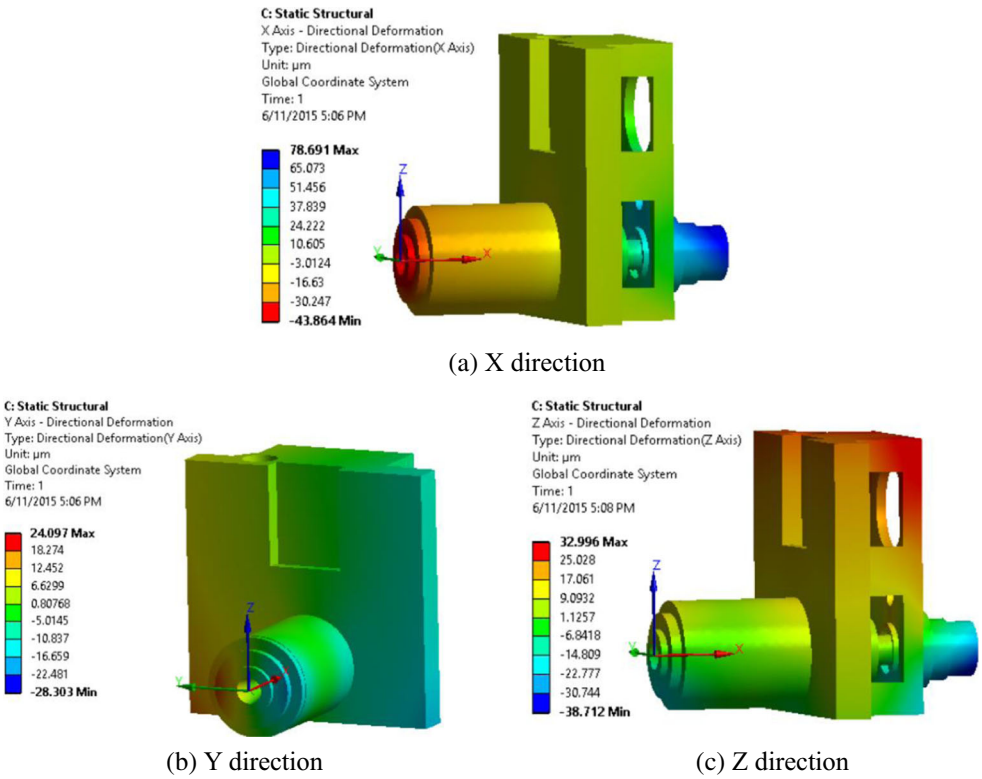


**Fig. 5** Simulated thermal error of the spindle at 2000 r/min (steady state)

From Fig. 5, we know that in the steady state the thermal errors in both Y and Z are 14.758 and 11.127 μm. Compared with those radial thermal errors, the thermal growth of the spindle (in X direction) is much bigger (38.271 μm).

### 3.2 Thermal key point selection

Thermal key points are defined as the points of which the temperature changes are closely related to the thermal error [6, 25]. The results of thermal key point selection are usually used as the guideline for placing the temperature sensors. And the temperatures of those points are often taken as the inputs of thermal error model. In order to find out the optimal points, kinds of methods such as the correlation analysis [26, 27], the group searching [28, 29], the gray system theory [30, 31], etc. are applied. In this paper, a new approach called mean impact valued (MIV) is proposed and used for selecting the thermal key points of the spindle system.

MIV is the index to evaluate the impact of independent variables on the dependent variables [32]. It is widely used in neural network modeling and analysis. According to the absolute value of MIV, inputs which are closely related to outputs of the neural network can be obtained. The main steps of MIV computation and variable selection are introduced as follows [33]:

1. The neural network is trained with original data.
2. The original input variables $P$ are increased and decreased of 10 % and two new samples $P_1$ and $P_2$ are obtained.
3. $P_1$ and $P_2$ are used as the inputs of well-trained neural network model, and two outputs $A_1$ and $A_2$ are obtained.

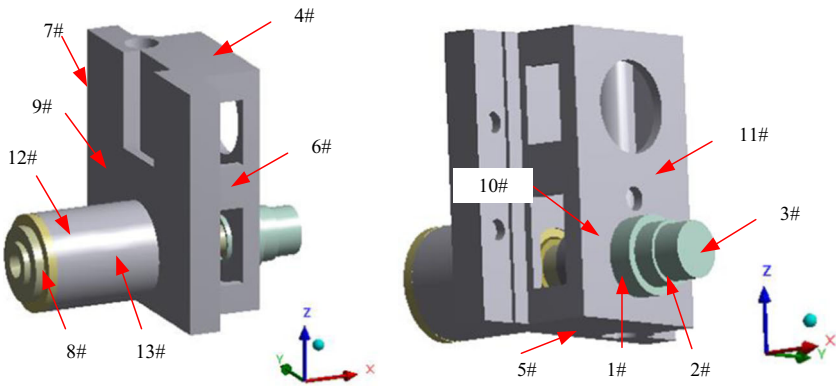


**Fig. 6** Candidates of the thermal key points in the spindle

**Table 5** MIV computation results and rank of candidate points

| Candidate points no. | MIV | Rank |
|---|---|---|
| 1 | 5.308429 | 4 |
| 2 | 2.425193 | 10 |
| 3 | 2.426116 | 9 |
| 4 | 3.294962 | 7 |
| 5 | 4.224264 | 6 |
| 6 | 4.433643 | 5 |
| 7 | 5.433654 | 3 |
| 8 | 1.490364 | 11 |
| 9 | 17.96691 | 1 |
| 10 | 0.195011 | 13 |
| 11 | 1.086334 | 12 |
| 12 | 2.818797 | 8 |
| 13 | 12.84348 | 2 |

4. The difference between $A_1$ and $A_2$ are calculated and named as the impact value (IV) of the input variables.
5. The impact values are divided by the number of samples and mean impact values (MIV) are obtained.
6. According to the absolute value of MIV, the input variables are sorted and the input variables which have great impact on the outputs are selected.

Based on the simulation results of the spindle temperature and the thermal error obtained in Section 1, 13 points in the spindle system are initially selected as the candidates. Their positions are shown in Fig. 6. 1# ~ 3# points are placed on the encoder as it is close to 3# bearing which has higher temperature rise. 4# ~ 7# points represent the temperature of the top, the bottom, the right, and the left surfaces of the spindle box. 8# point is located at the front end of the spindle. On the front surface, we select one point (9#), but on the back surface we select two points (10# and 11#). Because the temperature of the bearings cannot be directly tested in practical, 12# and 13# are placed at the points on the surface of the spindle nose. The positions of 12# and 13# points are corresponded to the positions of 1# and 2# bearings, respectively.

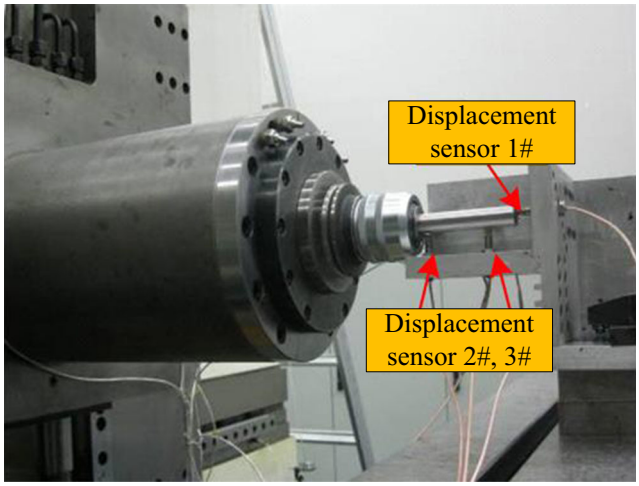


**Fig. 8** Measurement of the thermal error of the spindle

Then, the MIV of these candidates are computed and sorted (Table 5).

According to Table 5, we select the first four points (9#, 13#, 7#, and 1#) as the thermal key points. They are renumbered as 1#, 2#, 3#, and 4# and their locations are shown in Fig. 7.

## 4 Experimental verification

### 4.1 Experiment setup

In order to verify the optimization results of heat convection coefficients and the results of thermal key point selection, experiments are implemented on a precision horizontal machining center. Besides the 13 candidates mentioned in Section 2.2 (Fig. 6), two more PT 100 temperature sensors are installed on the motor and the bed. They are used to test the temperature change of the motor (another heat source) and the temperature fluctuation of the environment as they have certain impacts on the temperature distribution of the spindle system.

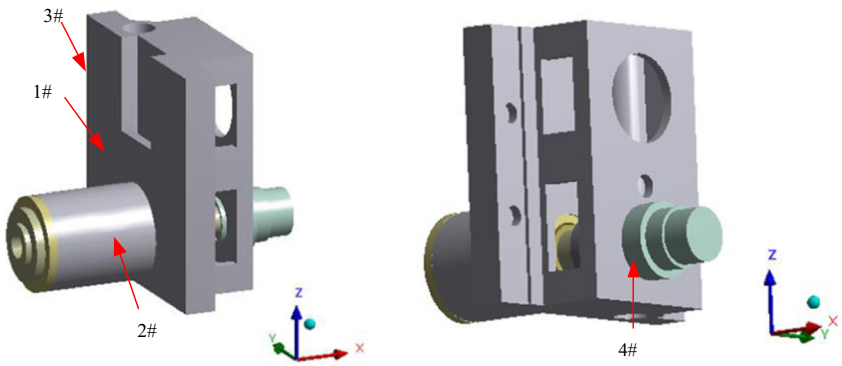


**Fig. 7** Positions of the thermal key points

**Table 6** Comparison of the simulation and testing results under different working conditions

| Spindle speed ($r \cdot min^{-1}$) | Optimization of heat convection coefficients | Encoder temperature (°C) | Error (%) | Spindle thermal error (μm) | Error (%) |
|---|---|---|---|---|---|
| 2000 | No | 33.541 | 2.89 | 38.271 | 9.97 |
| | Yes | 32.353 | 0.76 | 37.636 | 8.15 |
| 3000 | No | 36.065 | 6.08 | 43.585 | 30.38 |
| | Yes | 38.15 | 0.65 | 49.049 | 21.65 |
| 4000 | No | 38.06 | 16.90 | 47.476 | 48.95 |
| | Yes | 43.624 | 4.75 | 64.402 | 30.75 |

According to ISO 2303, a spindle thermal error testing system including three displacement sensors is constructed. This system is used to measure the axial and radial thermal error of the spindle. But in this paper, only the thermal growth is studied because the thermal errors in axial direction are much bigger than the radial ones. Figure 8 shows the setup of the spindle axial thermal error tests.

In this paper, three different tests numbered from 1 to 3 under different working conditions are conducted. In these tests, the spindle is running at 2000, 3000, and 4000 r/min until the temperatures and the thermal error reach to the steady state.

### 4.2 Verification for the optimization of convection heat transfer coefficients

In order to verify the results of convection heat transfer coefficients optimization, the simulated temperature of the encoder and the axial thermal error of the spindle before and after the optimization are compared with the experimental data. The measured encoder temperatures are 32.6, 38.4, and 45.8 °C, while the tested axial thermal errors are 34.8, 62.6, and 93 μm at 2000, 3000, and 4000 r/min, respectively. The comparison results are listed in Table 6.

From Table 6, it can be seen that the temperature simulation results are satisfying; after heat convection coefficients optimization, the errors between the simulated values and the experimental data are less than 5 %. And after optimization of heat convection coefficient, the errors between the simulation temperature and experimental data (2000 r/min) are decreased from 2.89 % to 0.76 %. While about 72 % errors of the simulated temperature at 4000 r/min is reduced after optimization. It means that the accuracy of simulation has been improved.

But there are big differences between the simulated and tested thermal errors. This is maybe because that when simulating the thermal error, the spindle system is considered as an independent system. The back face of the spindle box is taken as a fixed and reference surface. The spindle thermal error is just related to the thermal deformations of components in the spindle system. However, in practical, the spindle system is connected to the skate and the column. When testing the thermal error at the tool point, thermal deformations of the skate and the column also have certain effects on the testing results. By simulating, we know that the thermal deformations of the

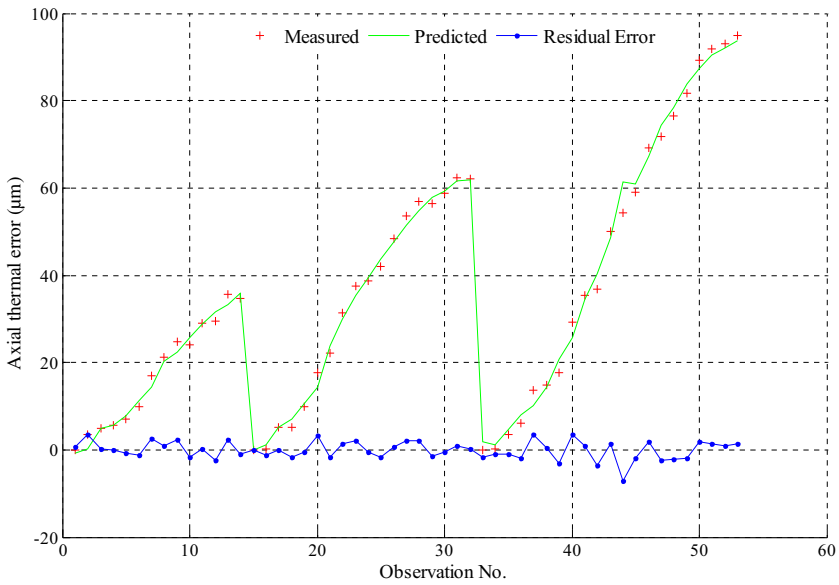


**Fig. 9** Results of BP modeling after the thermal key point selection

**Table 7** Comparison of the thermal error modeling before/after the thermal key point selection

| Model no. | Thermal key point selection | BP modeling | | |
|---|---|---|---|---|
| | | Minimum error (μm) | Maximum error (μm) | MSE |
| 1 | No | −7.4959 | 7.4671 | 11.3801 |
| 2 | Yes | −6.2236 | 3.5677 | 4.2119 |

skate and the column in the axial direction of the spindle are in range of [0, 30 μm] and [0, 12 μm]. Although the accuracy of the thermal error simulation is not perfect, it can also be concluded from Table 6 that after the optimization, the accuracy is improved.

### 4.3 Verification for the thermal key point selection

Referring to [34], the temperature of the thermal key points, the spindle speed, the historical information, and the time lag are taken as the input variables and axial thermal errors are taken as the output. By using BP neural network, the spindle thermal error models are developed. The modeling results are shown in Fig. 9. By comparing the results of modeling before and after the thermal key point selection (Table 7 and Fig. 10), the correctness and effectiveness of the selection are verified. MSE in Table 7 denotes the mean square errors.

According to Table 7 and Fig. 10, the residual errors between the experimental data and modeling results after the thermal key point selection are in the range of −7 to 4 μm. While before the thermal key point selection, the residual errors lie between −8 and 8 μm. In addition, MSE of model 2 is only about 37 % of model 1. It means that the model built on the temperatures of the thermal key points has better accuracy.

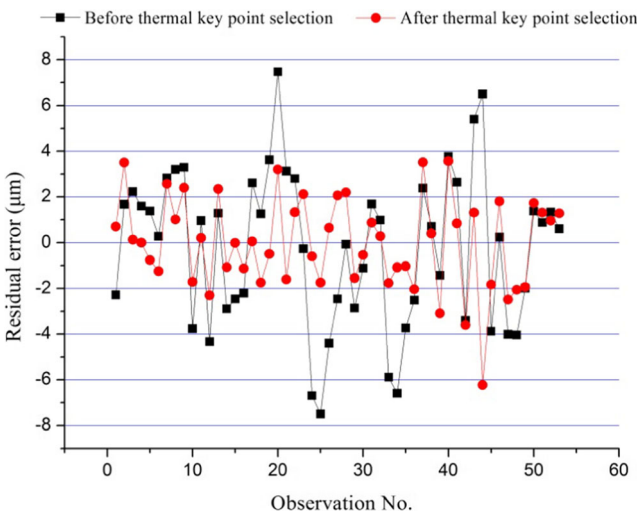


**Fig. 10** Residual errors of modeling before and after the thermal key point selection

## 5 Conclusions

The coefficients of convection heat transfer were regarded as the primary boundary conditions when simulating the temperature field and thermal error of the spindle system by finite element analysis. Aiming at improving the FEA accuracy, those coefficients were optimized based on the inverse heat conduction theory by using response surface methodology. By comparing the simulation results with the measured data which were collected from a precision horizontal machining center, it can be concluded that after optimization the FEA accuracy was improved.

Based on the simulation results, a new method named mean impact value was used for selecting the thermal key points and four thermal key points were selected from 13 candidates. By using the temperatures of selected thermal key points, the motor temperature, the environmental temperature, the spindle speed, historical information, and the time lag as the inputs, the thermal error model of the spindle on the precision horizontal machining center was established. The modeling result indicated that after the thermal key point selection, the accuracy of the model was improved. In other words, using the temperature data obtained from the thermal key points for the thermal error modeling and compensation would save the energy and guarantee the modeling accuracy at the same times.

**Acknowledgments** It is gratefully acknowledged that the work has been supported by the State Key Laboratory for Manufacturing System Engineering (China) and National Science and Technology Major Project of China (2014ZX04014021).

## References

1. Ramesh R, Mannan M, Poo A (2000) Error compensation in machine tools—a review: part I: geometric, cutting-force induced and fixture-dependent errors. Int J Mach Tools Manuf 40(9):1235–1256
2. Mancisidor I, Zatarain M, Munoa J, Dombovari Z (2011) Fixed boundaries receptance coupling substructure analysis for tool point dynamics prediction. Adv Mater Res 223:622–631
3. Huang Y, Zhang J, Li X, Tian L (2014) Thermal error modeling by integrating GA and BP algorithms for the high-speed spindle. Int J Adv Manuf Technol 1–7
4. Bryan J (1990) International status of thermal error research (1990). CIRP annals-manufacturing technology 39(2):645–656

5. Sarhan AA (2014) Investigate the spindle errors motions from thermal change for high-precision CNC machining capability. Int J Adv Manuf Technol 70(5–8):957–963
6. Li Y, Zhao W, Lan S, Ni J, Wu W, Lu B (2015) A review on spindle thermal error compensation in machine tools. International Journal of Machine Tools & Manufacture 95:20–38
7. Creighton E, Honegger A, Tulsian A, Mukhopadhyay D (2010) Analysis of thermal errors in a high-speed micro-milling spindle. Int J Mach Tools Manuf 50(4):386–393
8. Li B, Hong J, Tian X (2016) Generating optimal topologies for heat conduction by heat flow paths identification. International Communications in Heat & Mass Transfer 75:177–182
9. Postlethwaite S, Allen J, Ford D (1999) Machine tool thermal error reduction—an appraisal. Proc Inst Mech Eng B J Eng Manuf 213(1):1–9
10. Uhlmann E, Hu J (2012) Thermal modelling of a high speed motor spindle. Procedia CIRP 1:313–318
11. Xiang S, Zhu X, Yang J (2014) Modeling for spindle thermal error in machine tools based on mechanism analysis and thermal basic characteristics tests. Proc Inst Mech Eng C: J Mech Eng Sci 0954406214531219
12. Chen D, Bonis M, Zhang F, Dong S (2011) Thermal error of a hydrostatic spindle. Precis Eng 35(3):512–520
13. Zhang J, Li H (2012) Thermal performance analysis for the machine tool's spindle. In: 2012 7th IEEE Conference on Industrial Electronics and Applications (ICIEA). pp 2131–2134
14. Ma X, Qiu J, Liu QW, Lin J (2012) Study on Spindle Thermal Field Distribution and Thermal Errors of Horizontal Machine Tool. In: Materials Science Forum. Trans Tech Publ, pp 273–276
15. Han J, Wang LP, Yu LQ (2010) Modeling and estimating thermal error in precision machine spindles. Applied Mechanics and Materials 34:507–511
16. Haitao Z, Jianguo Y, Jinhua S (2007) Simulation of thermal behavior of a CNC machine tool spindle. Int J Mach Tools Manuf 47(6): 1003–1010
17. Alifanov OM (2012) Inverse heat transfer problems. Springer Science & Business Media
18. Ozisik MN, Orlande H, Kassab AJ (2002) Inverse heat transfer: fundamentals and applications. Appl Mech Rev 55(1):B18
19. Wang G, Zhu L, Chen H (2011) A decentralized fuzzy inference method for solving the two-dimensional steady inverse heat conduction problem of estimating boundary condition. International Journal of Heat & Mass Transfer 54(13):2782–2788
20. Baş D, Boyacı İH (2007) Modeling and optimization I: usability of response surface methodology. J Food Eng 78(3):836–845
21. Liu Y-T, Zhang L (2016) An investigation into the aspheric ultraprecision machining using the response surface methodology. Precis Eng 44:203–210. doi:10.1016/j.precisioneng.2015.12.006
22. Lienhard JH (2013) A heat transfer textbook. Courier Corporation
23. Li Y, Zhao W Axial thermal error compensation method for the spindle of a precision horizontal machining center. In: Mechatronics and Automation (ICMA), 2012 International Conference on, 2012. IEEE, pp 2319–2323
24. Harris T (1991) Rolling bearing analysis. Willey, New York
25. Guo Q, Yang J, Wu H (2010) Application of ACO-BPN to thermal error modeling of NC machine tool. Int J Adv Manuf Technol 50(5–8):667–675
26. Vyroubal J (2012) Compensation of machine tool thermal deformation in spindle axis direction based on decomposition method. Precis Eng 36(1):121–127
27. Weck M, McKeown P, Bonse R, Herbst U (1995) Reduction and compensation of thermal errors in machine tools. CIRP Annals-Manufacturing Technology 44(2):589–598
28. Lo C-H, Yuan J, Ni J (1999) Optimal temperature variable selection by grouping approach for thermal error modeling and compensation. Int J Mach Tools Manuf 39(9):1383–1396
29. Han J, Wang L, Wang H, Cheng N (2012) A new thermal error modeling method for CNC machine tools. Int J Adv Manuf Technol 62(1–4):205–212
30. Li Y, Yang J, Gelvis T, Li Y (2008) Optimization of measuring points for machine tool thermal error based on grey system theory. Int J Adv Manuf Technol 35(7–8):745–750
31. Yan J, Yang J (2009) Application of synthetic grey correlation theory on thermal point optimization for machine tool thermal error compensation. Int J Adv Manuf Technol 43(11–12):1124–1132
32. Jiang JL, Su X, Zhang H, Zhang XH, Yuan YJ (2013) A novel approach to active compounds identification based on support vector regression model and mean impact value. Chem Biol Drug Des 81(5):650–657
33. Zhong-guang F, Min-fang Q, Yuan J (2012) Regression forecast of main steam flow based on mean impact value and support vector regression. In: Power and Energy Engineering Conference (APPEEC), 2012 Asia-Pacific. pp 1–5. doi:10.1109/APPEEC.2012.6307580
34. Li Y, Zhao W, Wu W, Lu B, Chen Y (2014) Thermal error modeling of the spindle based on multiple variables for the precision machine tool. Int J Adv Manuf Technol 72(9–12):1415–1427. doi:10.1007/s00170-014-5744-4